Magnetorheological-Actuators: An Enabling Technology for Fast, Safe, and Practical Collaborative Robots

Alexandre St-Jean, Francis Dorval, Jean-Sébastien Plante, and Alexis Lussier-Desbiens

***Abstract*—Collaborative robots are more and more used in applications requiring robots and humans to work in proximity or direct contact. However, conventional collaborative robots powered by servo-geared actuators are intrinsically dangerous due to their high reflected inertia. Recent studies have shown that low inertia and high bandwidth (>30 Hz) magnetorheological (MR) actuators have the potential to improve the safety of collaborative robots without reducing their force and speed capabilities. The main contribution of this article is to provide a quantitative assessment of how MR actuators can contribute to reducing the impact forces with humans, and thus increase the safety of collaborative robots. Dynamic models, validated with simplified 1 degrees-of-freedom (experiments, show that the safety level of collaborative robots can be increased by a factor up to 3 only by changing the conventional servo-geared actuator architectures for MR actuators with no other changes. The article also presents a simple, reliable, and fast collision detection method based on joint angular velocity band-pass filtering, a method exploiting the unique low inertia and clean dynamics properties of MR actuators. Finally, an experimental comparison of representative collaborative robots demonstrates an impact force reduction of 10 times using MR actuators, fast collision detection, and passive foam padding.**

***Index Terms*—Collaborative robots, collision detection, magnetorheological (MR) clutch, robot architectures, robot safety.**

I. Introduction

OVER the past decades, industrial robots have become the standard on assembly lines in many industrial sectors with their ability to travel at very high speeds (e.g., up to 3 m/s at the end-effector) while maintaining a high positioning accuracy (e.g., <1 mm). Such manipulators can perform dangerous and repetitive tasks better than humans such as welding, machining, and positioning heavy components on assembly lines. However, industrial robots are massive and nonbackdriveable resulting in lethal risks in the event of unwanted contact with humans. As a result, industrial robots must be placed in safe zones such as metallic cages to guarantee safety [1].

Recently, labor shortage drove the development and commercialization of easy-to-use *collaborative* robots that can work alongside human coworkers in a multitude of new industries while being human-safe. The versatility of collaborative robotics will allow robots to do more nontraditional tasks while being close to people. They will also reduce the risk of work accidents, increase the flexibility of robotic stations, and help reduce the cost per part of low-volume production [2], [3].

The mechanical design of collaborative robots must be intrinsically safe to effectively perform tasks close to humans, [4], [5]. The vast majority of today's collaborative robots use electromagnetic motors coupled to high-reduction gearboxes in a one-per-joint architecture. These designs impose performance tradeoffs to remain safe due to the high reflected inertia of dc motors resulting from the high reduction gearboxes. Indeed, today's collaborative robots must be slowed down, have limited force outputs, and use serial elastic components to absorb collision energy and remain safe [6], [7], [8], [9]. As a result, collaborative robots are slower, less powerful, less precise, and more sensitive to disturbances than traditional industrial robots.

Another aspect of safe human–robot collaboration is the fast and reliable detection of collisions. Cameras, laser scanners, and instrumented robot skins can be used to detect the proximity or contact between a human and a robot, but these techniques require heavy calculations and complex hardware, resulting in poor real-time performance, low reliability, and increased costs [10], [11]. An alternative to sensorial feedback is model-based collision detection schemes, such as external torque observers that can detect collisions by comparing commanded to expected torque [12]. However, model-based approaches are highly dependent on the precision of the dynamic model which is challenging for servo-geared motors due to nonlinear phenomena such as friction, transmission elasticity, and backlash [13], [14]. Yet another alternative is the use of costly instrumentation such as joint torque sensors at each joint, again at the sacrifice of costs, weight, and reliability.

In addition to the ability to detect collisions reliably and rapidly, a proper postimpact reaction strategy is needed to minimize damage to humans and robots. Different reaction strategies or reflex motions, such as gravity compensation or reflex torque, have been implemented in collaborative robots [14] and exhibit

Manuscript received 19 May 2023; revised 9 October 2023; accepted 7 November 2023. Date of publication 12 December 2023; date of current version 10 January 2024. This paper was recommended for publication by Associate Editor A. Dietrich and Editor M. Yim upon evaluation of the reviewers' comments. This work was supported in part by NSERC, in part by FRQNT, in part by CSA, in part by the Canada Research Chair Program, in part by the NSERC-CREATE CoRoM program (www.corom.ca), in part by the IRSST, and in part by Exonetik. *(Corresponding author: Alexandre St-Jean.)*

The authors are with the Faculty of Engineering, Mechanical Engineering Department, Université de Sherbrooke, Sherbrooke, QC J1K 0A5, Canada (e-mail: alexandre.st-jean3@usherbrooke.ca; francis.dorval@usherbrooke.ca; jean-sebastien.plante@usherbrooke.ca; alexis.lussier.desbiens@usherbrooke.ca).

This article has supplementary downloadable material available at https://doi.org/10.1109/TRO.2023.3341573, provided by the authors.

Digital Object Identifier 10.1109/TRO.2023.3341573

acceptable force reduction at low speeds (i.e., < 1 m/s). The main limitation for faster reaction rates when using reactive strategies is the low actuator force bandwidth caused by the high inertia from the high transmission ratio found in conventional servomotor and gearbox actuators.

Regardless of their collision mitigation strategy, current collaborative robots must demonstrate that contact forces always remain within the guidelines exposed in ISO/TS 15066 [15]. Consequently, the widespread adoption of collaborative robot systems is impeded by actuation technology limitations preventing operation at human-like speeds while being safe.

Recent research suggests that actuators based on magnetorheological (MR) fluid could be less sensitive to the performance/safety tradeoff impeding collaborative robotics [16]. These actuators transmit torque through a rotary clutch filled with magnetorheological fluid. The fluid's viscosity, and thus transmitted shear stresses, can be varied as a function of the magnetic field passing through it. Having a fluid layer significantly reduces the perceived inertia by detaching the inertia of the highly geared dc motor driving the clutch from the actuator output. Output inertia is significantly reduced by one to two orders of magnitude resulting in increased bandwidth and transparency [17], [18], [19], [20], [21], [22]. By removing undesirable inertial loads, MR actuators allow better dynamic performances (i.e., speed, power, strength, and precision) while being intrinsically safer by storing little kinetic energy and momentum in fast-stop scenarios such as collisions [23]. These advantages can be magnified by the use of a proper transmission system to further reduce the inertia of the arm, such as tendons [17] or leader/follower hydrostatic systems [20]. MR actuators also avoid direct mechanical contact between transmission components in emergency stop situations, thanks to the fluid interface, thus limiting loads leading to actuator failures or long mechanical clamping in human–robot collisions.

Even if actuator architecture (i.e., the mechanical design of the actuators and transmission) is crucial in determining the safety level of human–robot operations [5], [7], [24], limited literature exists on the topic. This article studies the potential of MR actuators for collaborative robot systems by providing a detailed and experimentally validated analysis of the effect of robot actuator technology and robot topology on impact force in collisions between robots and humans. The low inertia of MR actuators, their high force bandwidth, and clean dynamics (e.g., no discontinuous, complex friction phenomenon, and no backlash) allow to revisit the three main components of a safe interaction between robots and humans cited previously, that is

1) an *intrinsically safer actuator architecture design* to reduce impact force in inevitable contact situations;
2) a *simple, model-less, reliable and fast collision detection;*
3) a *fast postimpact reaction*.

The rest of this article is organized as follows. Section II presents a reduced-order analytical model along with an experimental comparison of MR actuators to traditional collaborative robot actuator architectures in terms of expected collision forces. Section III presents a sensorless and model-less, collision detection scheme exploiting the clean dynamics of MR actuators and leading to a simple and robust collision detection approach.

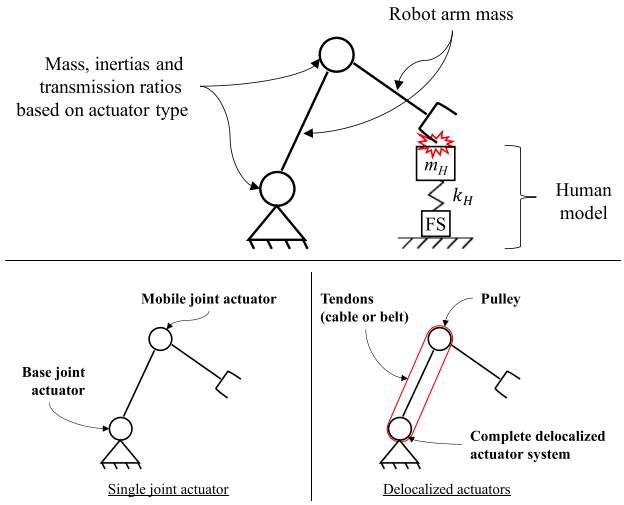

Fig. 1. Impact model and actuator architectures schematics (single joint versus delocalized actuators).

Section IV presents an experimental comparison of the collision performance of a 3 degrees-of-freedom (DOF) collaborative robot powered with MR actuators and a universal robot UR5 collaborative robot powered with conventional actuators. The comparison is made in a representative work environment and includes scenarios where collisions are made with and without foam padding. In Section V, an attempt is made to push the available hardware to its physical limits. Finally, Section VI concludes this article.

II. Intrinsic Impact Force Reduction

A. Impact Model and Architecture Comparison

A generic 2 DOF model of a robotic manipulator impacting a clamped human is developed to compare the resultant impact forces produced by relevant robot actuator architectures. The clamped (or constrained) collision, see Fig. 1, is selected because it represents a major portion of injuries occurring between humans and robots [25], [26]. The human portion of the model is represented by a mass-spring model with mass m_H and stiffness k_H extracted from ISO/TS 15066 [15], instrumented with a force sensor. The mass-spring is set to represent a human hand (0.6 kg and 75 N/mm, respectively) as it is the most stringent condition of ISO/TS 15066 for a clamped impact (the hand condition is used everywhere in this article).

Actuator mass and inertia of architectures of interest are used to evaluate impact forces for given end-effector speeds and joint angle configurations. To do so, the reflected effective mass of the manipulator at the end-effector from the actuator inertia m_A and from the link masses and inertia m_L, along with collision direction is evaluated by reporting the kinematics of each component at the end-effector [27]

$$\frac{1}{m_A} = \boldsymbol{u}^T \boldsymbol{J}(\boldsymbol{q}) \boldsymbol{M}_A(\boldsymbol{q})^{-1} \boldsymbol{J}^T(\boldsymbol{q}) \boldsymbol{u} \tag{1}$$

$$\frac{1}{m_L} = \boldsymbol{u}^T \boldsymbol{J}(\boldsymbol{q}) \boldsymbol{M}_L(\boldsymbol{q})^{-1} \boldsymbol{J}^T(\boldsymbol{q}) \boldsymbol{u} \tag{2}$$

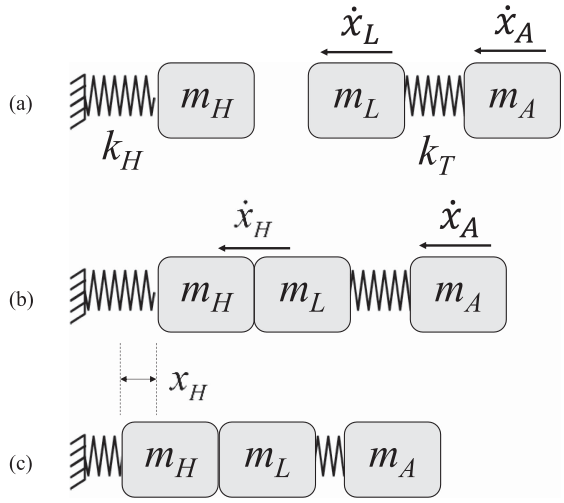

Fig. 2. 1-D collision model when masses are (a) preimpact, (b) at the instant of impact, and (c) postimpact where maximal force is reached.

where $\boldsymbol{q}$ is the angular joint position vector, $\boldsymbol{u}$ the contact direction, $\boldsymbol{J}$ the Jacobian matrix, $\boldsymbol{M_A}$ the manipulator actuator inertia matrix, and $\boldsymbol{M_L}$ the manipulator links and structure inertia matrix.

Then, the contact is evaluated as a one-dimensional (1-D) collision in the contact direction with the initial robot velocity $\dot{x}_A = \dot{x}_L$, see Fig. 2. The transmission between the actuator and the link is modeled with a spring of stiffness k_T. The assumptions that the robot's and human's masses stay together, and that kinetic energy is entirely absorbed in the spring compression x_H represent the worst possible case for maximal impact force as presented in ISO/TS 15066. It shall be seen as the safest evaluation of potential damage that can occur to humans.

Rigid bodies conservation of momentum p during collision is used to determine postimpact velocity $\dot{x}_H$ of the combined robot link equivalent mass and human body part's mass in the contact direction

$$p = m_L\dot{x}_L = (m_L + m_H)\dot{x}_H \tag{3}$$

$$\dot{x}_H = \left(\frac{m_L}{m_L + m_H}\right)\dot{x}_L. \tag{4}$$

Postimpact velocity allows to calculate the maximum compression of the spring representing the human, and thus the maximum collision force. This conservative scenario assumes that the kinetic energy of the masses at the moment of the impact E_K is completely converted to potential energy of the spring E_S at maximum deflection (i.e., no kinetic energy and no potential energy is stored in m_A and k_T when the maximal force occurs)

$$E_K = \frac{1}{2}(m_L + m_H)\dot{x}_H^2 + \frac{1}{2}m_A\dot{x}_A^2 \tag{5}$$

$$E_S = \frac{1}{2}k_H x_H^2. \tag{6}$$

The force F_H produced by the spring compression is evaluated knowing the compression and stiffness of the spring [15]

$$F_{H,\max} = k_H x_{H,\max}. \tag{7}$$

By combining (4)–(7), it is possible to express the maximal contact force as a function of the human stiffness, human mass, the equivalent masses of the robot, and robot cartesian velocity in contact direction

$$F_{H,\max} = \dot{x}_A\sqrt{k_H\left(\frac{m_L^2}{m_L + m_H} + m_A\right)}. \tag{8}$$

The performance of various actuator architectures during collision is compared based on a *speed ratio*. The speed ratio is the ratio of the end-effector speed producing the same maximum contact force as a reference configuration. The reference configuration is taken as a 50:1 harmonic gearbox coupled to a dc motor since this is an actuator architecture similar to the popular UR5. The speed ratio relationship is found by setting the same impact force

$$F_{H,1} = F_{H,2} \tag{9}$$

$$\dot{x}_{A,1}\sqrt{k_H\left(\frac{m_L^2}{m_L + m_H} + m_{A,1}\right)} = \dot{x}_{A,2}\sqrt{k_H\left(\frac{m_L^2}{m_L + m_H} + m_{A,2}\right)} \tag{10}$$

$$\text{speedratio} = \frac{\dot{x}_{A,1}}{\dot{x}_{A,2}} = \sqrt{\frac{m_L^2 + m_{A,2}(m_L + m_H)}{m_L^2 + m_{A,1}(m_L + m_H)}}. \tag{11}$$

Note that the *speed ratio* has a *force ratio* counterpart but, in this case, at the same impact speed. A *speed ratio* of "X" at the same impact force implies a *force ratio* of "1/X" at the same impact speed.

It is well known that introducing transmission compliance between the actuator and the robot links (e.g., with serial-elastic actuators) helps reduce collision force by distributing the impact over time [9]. The *speed ratio* presented in (11) offers a simple, yet conservative way of comparing two robot architectures because the effect of transmission compliance in force distribution over time is not accounted for. To quantify this effect, the dynamic equations of the three masses of the model presented in Fig. 2 [see (12)–(14)] can be solved numerically with the same masses used to simulate maximal force with representative actuator stiffness. The contact stiffness between m_L and m_H is modeled as a stiff spring k_C (10x k_H) that can only apply compressive forces. The *speed ratio* can then be evaluated with the inverse ratio of the maximal forces as calculated with (7)

$$m_H\ddot{x}_H = k_C(x_L - x_H) - k_H x_H \tag{12}$$

$$m_L\ddot{x}_L = k_T(x_A - x_L) - k_C(x_L - x_H) \tag{13}$$

$$m_A\ddot{x}_A = -k_T(x_A - x_L). \tag{14}$$

Simulation results of the impact of the 2 DOF robot of Fig. 1 with two 110 N·m joint torque capacity are presented in Table I using 1) the numerical simulation of (12)–(14) (labeled SIMULATION), and 2) the simple evaluation of the *speed ratio* of (11) based on the human spring elastic energy (labeled ENERGY).

Actuator masses and inertias (model inputs) come from torque-to-weight and torque-to-inertia correlations extracted

TABLE I
SPEED RATIO OF MOST COMMON ACTUATOR ARCHITECTURES FOR A 2-DOF ROBOT WITH 110 NM PER JOINT

Architecture	*Performance metrics*				
	Rank (Sim)	*Speed ratio (Sim)*	*Speed ratio (Energy)*	*Actuators mass [kg] (Increase from ref.)*	
(A) MR Delocalized with 1:1 Hydrostatic transmission	*1*	*2.30*	*2.55*	*18.9*	*(3.6x)*
(B) MR Delocalized with 1:1 Tendons	*2*	*2.16*	*2.74*	*18.3*	*(3.4x)*
(C) MR Delocalized with 6:1 Tendons	*3*	*2.06*	*2.09*	*8.3*	*(1.6x)*
(D) MR Delocalized with 6:1 Hydrostatic transmission	*7*	*1.49*	*1.57*	*8.9*	*(1.7x)*
(E) MR At joint with 1:1 Direct transmission	*5*	*1.86*	*2.24*	*20.8*	*(3.9x)*
(F) MR At joint with 6:1 Planetary gearbox	*6*	*1.50*	*1.79*	*8.6*	*(1.6x)*
(G) DC Delocalized with 1:1 Tendons transmission	*3*	*2.06*	*2.14*	*50.7*	*(9.6x)*
(H) DC Delocalized with 50:1 Tendons and Planetary gearbox	*8*	*1.43*	*1.10*	*7.1*	*(1.3x)*
(I) DC Delocalized with 160:1 Tendons and Planetary gearbox	*9*	*1.02*	*0.66*	*5.8*	*(1.1x)*
(J) DC At joint with 50:1 Harmonic gearbox (REFERENCE)	*10*	*1.00*	*1.00*	*5.3*	*(1x)*
(K) DC At joint with 50:1 Planetary gearbox	*11*	*0.98*	*0.98*	*6.9*	*(1.3x)*
(L) DC At joint with 160:1 Harmonic gearbox	*12*	*0.69*	*0.66*	*4.0*	*(0.8x)*
(M) DC At joint with 160:1 Planetary gearbox	*13*	*0.66*	*0.62*	*5.6*	*(1x)*

from a large database of more than 400 commercially available actuation components including dc motors (e.g., Frameless Kollmorgen, brushless Maxon, 0.5 to 11.1 N·m), planetary gearboxes (e.g., Maxon gearhead, 12:1 to 756:1 ratio, 3 to 120 N·m output), and harmonic gearboxes (e.g., HarmonicDrive HFUS/HPG series, 30:1 to 160:1 ratio, 6.8 to 216 N·m output) and MR clutches (e.g., existing designs, 0.4 to 75 N·m output). The actuator components are scaled using scaling laws presented in [28]. Actuator architecture's masses and inertias are estimated by combining the adequate components for a given joint design. For example, the "dc At joint with 50:1 Planetary gearbox transmission" configuration includes the sum of the masses and inertias for a 110 N·m output planetary gearbox and a brushless dc motor of 2.2 N·m located at the joints. Robot links masses and inertias are modeled as aluminum cylinders (75 mm diameter, 400 mm long, 3 mm thick) similar to collaborative robots of 5 kg nominal payload.

Results in Table I are sorted by configuration group, and then by speed ratio within their group (evaluated with the dynamic simulation method). Respectively, the architecture groups are MR with delocalized actuators (A to D), MR with actuators at the joints (E to F), dc with delocalized actuators (G to I), and dc with actuators at the joints (J to M). Delocalized architectures are designs where all actuators are located in the base of the robot and the joints are remotely actuated by a low inertia transmission, thus reducing the mobile mass. In contrast, "At joint" architectures have actuators directly located at the joints. Table I also presents the total mass of the complete actuation system for each scenario.

Simulation results predict that architectures with MR actuators have higher speed ratios (i.e., 1.5 to 2.7) than conventional harmonic geared architectures (i.e., 0.7 to 1.0). For "at joint" MR configuration, significant mass reduction of these MR architectures can be realized with a lightly geared transmission after the MR clutch output with a small effect on speed ratio (e.g., 6:1 MR architecture).

It is also possible to observe in Table I that the delocalized dc motor with direct (i.e., 1:1) tendons transmission (Architecture G) has a good speed ratio of 2.1. However, even for a 2 DOF robot, this architecture results in a heavy robot with 50.7 kg of actuator mass. This will lead to an unpractical payload-to-mass ratio that can be prohibitive in many applications such as manipulators on mobile bases and field robotics where weight reduction is crucial.

It can also be observed that the delocalization of dc actuators with a high gearbox ratio only gives marginal gains with the energy-based model compared to the architecture with the same actuators located at joints because the reflected inertia of the actuators is dominant in determining the impact force. However, these delocalized dc configurations perform slightly better when considering the compliant cable transmission.

Finally, for a given reduction ratio, architectures composed of planetary and harmonic gearboxes have different speed ratios because of the slight difference in the inertia of the gearbox [28]. In practice, harmonic gearboxes are often preferred for other considerations, like their low backlash and lower mass. However, in both types of gearboxes, the higher reduction ratio is detrimental to safety because of the increased reflected inertia.

The *speed ratio* is defined here as the performance metric to allow simple comparisons between robot architectures solely based on maximal impact force estimation from robot inertial parameters (as suggested in ISO/TS 15066), which dominates safety [29], without consideration of the potential injuries that could result from impacts. This metric is used, as opposed to collision metrics from the automotive industry [e.g., head injury criterion (HIC)] since they are irrelevant in a clamped impact scenario because the impacted human body parts cannot move significantly, and thus cannot gain high velocity or acceleration. Furthermore, as demonstrated in [25], even for unconstrained impact with heavy industrial robots, metrics from the automotive industry based on high accelerations and velocities like the HIC are not appropriate to measure injuries in human–robot interaction.

B. Experimental Validation on a Single Actuator

An experimental 1 DOF test bench is built with similar mass and inertia found on commercial collaborative robot arms (e.g., UR5 arm without actuators, equivalent mass of 2.0 kg and 3.7E-2 kg·m^2 about pivot axis) to verify simulation results, see Figs. 3 and 4. The arm is driven by two different actuator technologies: 1) an ElectroCraft RP34-112 brushless dc motor (1.2 N·m at 4800 r/min) geared with an Applied Motion 34VL050 50:1 planetary gearbox with an equivalent rotational stiffness estimated at 2 kNm/rad (limited by the 12 mm arm shaft); and 2) the same ElectroCraft RP34-112 brushless dc motor geared with a

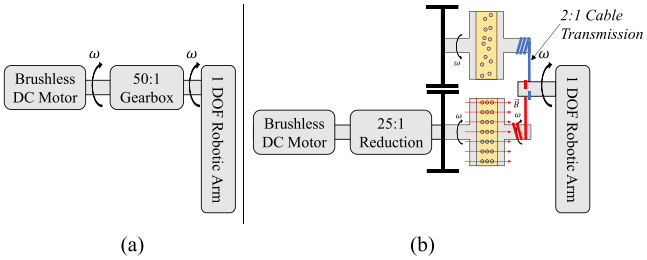

Fig. 3. Schematic of (a) dc motor and planetary gearbox, and (b) MR actuator and tendons transmission architecture of 1 DOF test bench.

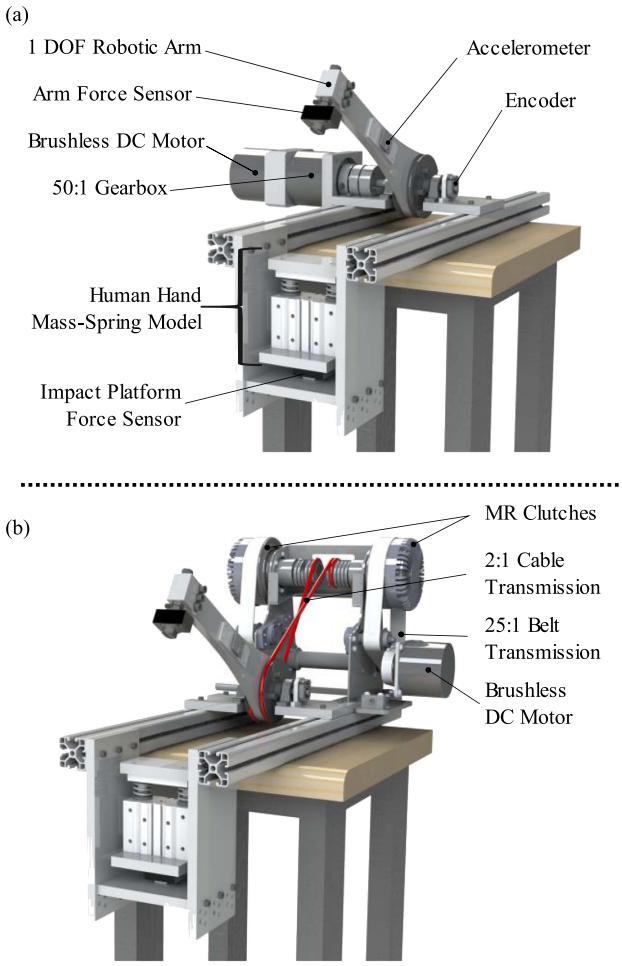

Fig. 4. Experimental 1 DOF impact test bench of (a) dc motor and planetary gearbox, and (b) MR actuator and tendons transmission.

25:1 gearbox and belts transmission connected to two custom antagonist 30 N·m MR clutches. Torque from the clutches is delivered to the arm through a 6 mm Dyneema SK75 2:1 cable transmission with an equivalent rotational stiffness estimated at 10 kNm/rad (limited by the cable). Both actuator systems are sized to develop a torque of 60 N·m at the joint with an angular velocity of 10 rad/s, corresponding to a 3 m/s tip speed. However, the output inertia of the conventional actuator is larger (3.04E-1 kg·m^2) by two orders of magnitude than the output inertia of the MR actuator (2.34E-3 kg·m^2).

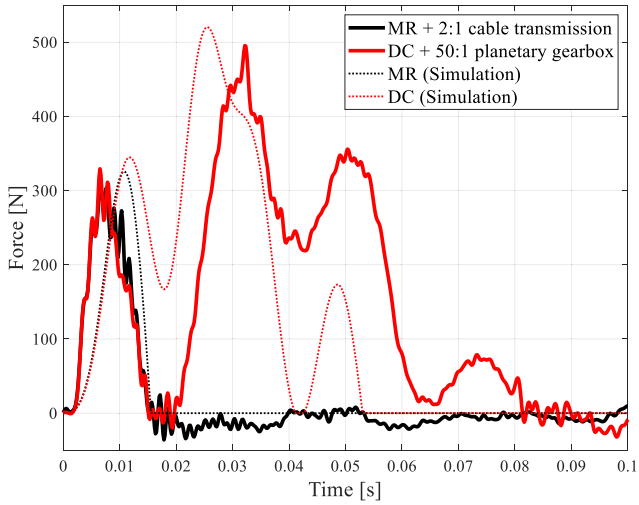

Fig. 5. Comparison of experimental impact force profile.

The experimental setup is equipped with two uniaxial force sensors, one at the tip of the arm and one under the mass-spring representing a human (0.6 kg and 75 N/mm respectively) to measure contact forces according to the ISO/TS 15066 [15]. The arm is also equipped with a +/– 50 g single-axis accelerometer (PCB Piezotronics 352C68) to detect contact and a 5000 pulses per revolution optical encoder at the joint for motion control and monitoring.

Experiments consist of taking the arm to an initial vertical position and then accelerating it to a tip speed of 2.5 m/s before contacting the human model. An impact detection strategy uses an acceleration threshold of 30 g at the impact point to trigger a reflex motion to return to a last known safe, preimpact position, here defined as the end-effector position 50 ms before contact. This position is selected here as a known safe target position for the sake of simplicity, but in a complete robot collision, this choice can lead to a possible secondary impact. The choice of position target should be taken by a higher level controller with environment constraints accounted for.

Contact force versus time signatures of both actuator technologies are shown in Fig. 5, along with simulated results using (12)–(14). Results show that MR actuators lead to a significant reduction in contact time and peak impact force. The predicted speed ratio between the two architectures is 1.59 (MR versus dc-planetary), whereas a speed ratio of 1.63 is measured experimentally from the inverse of the ratio of maximal impact forces. The experimental setup actuator equivalent masses and stiffness at the impact point are $m_L = 0.45$ kg (same for both actuators), $m_{A,\mathrm{DC}} = 2.9$ kg, $k_{T,\mathrm{DC}} = 19$ kN/m, $m_{A,\mathrm{MR}} = 0.026$ kg, $k_{T,\mathrm{MR}} = 110$ kN/m.

The small differences in time distribution of the impact are explained by unmodeled phenomena such as distributed mass and compliance resonance inside the actuator, link pivot friction, and backlash for the geared dc actuator. One can see in Fig. 5 by analyzing the force versus time plot that the initial portion of the impact is similar for both actuators since it is dominated by the link inertia. However, after the initial contact phase (0–20 ms),

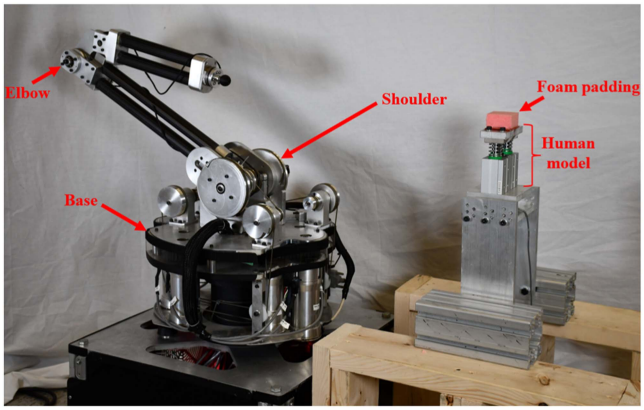

Fig. 6. MR robot Asimov with delocalized actuators and tendons transmission.

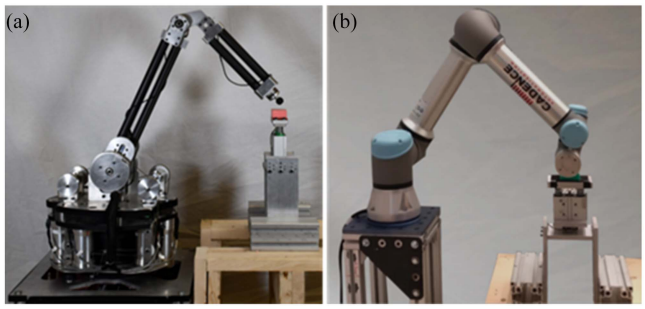

Fig. 7. Configuration at impact for (a) Asimov MR robot, and (b) Universal Robot UR5.

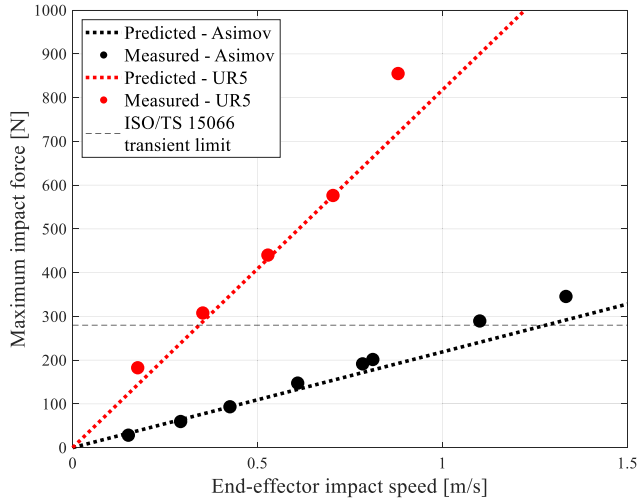

Fig. 8. Measured and predicted maximum impact force as a function of end-effector impact speed for Asimov and UR5 (see Fig. 15 no foam, for Asimov 1 m/s and UR5 0.88 m/s temporal plots of impact force).

the larger inertia of the dc actuator continues to compress the transmission spring and produces a longer collision. The peak impact force reached near 30 ms is thus mainly driven by the actuator inertia. This explains why the MR actuator does not have a secondary impact phase, since the actuator inertia is an order of magnitude smaller than the link inertia and does not compress the transmission significantly to apply a significant force on the link.

The multimodal force plot of Fig. 5 highlights that for robot actuators with distributed stiffness (e.g., 20 kNm/rad) and inertia similar to actual collaborative robot actuators, not only the initial impact should be considered in a safety analysis, but the complete dynamic parts. Secondary impacts in clamped scenario caused by a particular combination of transmission stiffness and inertia can produce larger forces than the initial impact typically considered in unconstrained free collisions.

C. Experimental Validation on Representative Robots

Model predictions for impact force and *speed ratio* are now verified by comparing the industry standard 6 DOF Universal Robot UR5 with a 3 DOF collaborative robot powered by MR actuators called Asimov (see Fig. 6). Asimov uses a single dc motor driving three pairs of antagonist MR clutches delivering torque to the three joints. All actuation components are delocalized in the base. Cable transmissions are used to route 27, 56, and 26 N·m torques to the base, shoulder, and elbow joints with post-clutch ratios of 4.2:1, 8.6:1, and 4:1, respectively. This architecture is similar to Architecture C presented in Table I. The robot's 0.9 m reach and 5 kg nominal payload were chosen to match the UR5. However, its nominal maximum effector speed is 4 m/s.

The same mass-spring human model as in the 1 DOF experiments is used at the point of impact of the collisions. The two robots are commanded with similar trajectories to reach a given end-effector speed at the point of impact. Note that the UR5 is limited to 0.88 m/s since higher impact speeds would be unsafe and would damage the joints.

Fig. 7 presents the angular configuration of the two robots at impact. The paths are designed to have a vertical impact in one plane, caused by a movement of the second and third joint only, as in the 2 DOF model of Fig. 1. This configuration was chosen as a representative position for a wide range of applications, such as a robot and an operator cooperating on the same table in a way that a robot picking up a component on the table could impact the operator's hand.

Fig. 8 shows impact force predictions for the Asimov and UR5 robots compared to experimental measurements. It can be observed that measurements correlate well with the prediction of the 1-D model of Section II-A ($R^2{}_{\text{Asimov}} = 0.924$, $R^2{}_{\text{UR5}} = 0.925$). The measured peak forces lead to a mean *speed ratio* of 3.81 between the two configurations, which is also very close to the model prediction of 3.85. The simulation equivalent masses and stiffness at the impact point for both robots are $m_{L,\text{UR}} = 1.42$ kg, $m_{A,\text{UR}} = 11.1$ kg, $k_{T,\text{UR}} = 130$ kN/m, $m_{L,\text{Asimov}} = 1.13$ kg, $m_{A,\text{Asimov}} = 0.044$ kg, $k_{T,\text{Asimov}} = 7.5$ kN/m. As demonstrated with the 1-DOF experiments, high transmission compliance does not contribute to significantly reducing the MR-actuated robot impact force, since the impact dynamic is highly dominated by structural inertia. Indeed, the energy-based model of (8) predicts an impact force of 242 N (951 N for the UR5), while the simulation using a compliant transmission predicts a force of 213 N (821 N for the UR5).

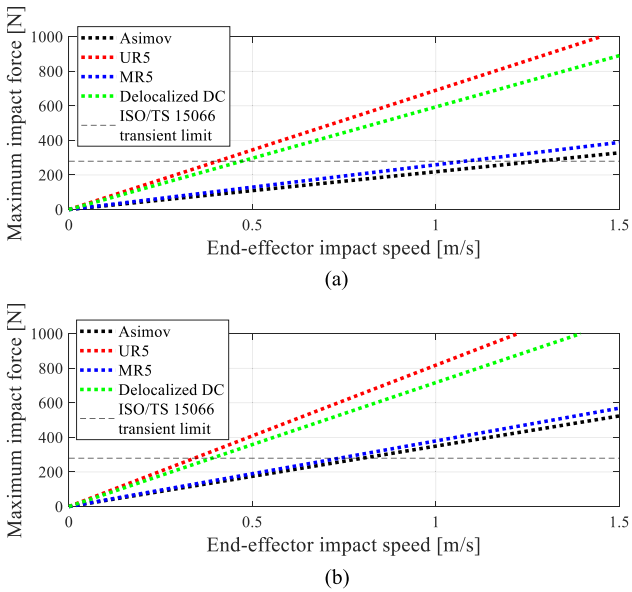

Fig. 9. Predicted maximum impact force as a function of end-effector impact speed for alternative robotic architectures of (a) 3 DOF (without wrist), and (b) 6 DOF (with wrist).

This comparison validates the model fidelity, and it can now be used to evaluate the safety level of robot architectures with high confidence. Since a direct comparison of Asimov and UR5 is unfair because of the different numbers of DOF. The next section presents a fair analysis, based on impact force model predictions and experimental data.

D. Model Predictions for Relevant Robot Architectures

Two design alternatives are considered, each for a 3 DOF and a 6 DOF configuration. These alternatives are used to highlights the effects of delocalization and actuation technology on safety.

1) The first one, *MR5*, is a robot with the same mechanical structure as UR5 but using MR actuators located at each joint.
2) The second one, *delocalized dc*, is a robot with the same lightweight mechanical structure as Asimov, but with UR5 actuators delocalized at the base of the robot.

The difference between the 3 and 6 DOF configurations is accounted for by adding or subtracting the UR5 wrist containing the 3 distal DOF as a point mass of 3.9 kg at the effector. Simulations from the 2 DOF model of the UR5 show that, when the wrist's mass is removed from UR5 (from 6 DOF to 3 DOF), contact forces are reduced by 15%, and when the wrist mass is added to Asimov (from 3 DOF to 6 DOF in a semi-delocalized way as in [30]), forces are augmented by 59%. Results are shown in Fig. 9 and derived speed ratios are listed in Table II. It can be concluded that:

1) Comparing the UR5 versus delocalized dc results shows that, regardless of the number of DOF, when using conventional actuators, actuator delocalization has limited benefits on safety. This reveals that actuator inertia is a more important design parameter than distributed mass for collaborative robots and must inevitably be minimized to gain significant safety benefits.
2) Results from 3 and 6 DOF UR5 and MR5 show that the benefits of using low inertia actuators are greater at low DOF since adding distal DOFs adds highly penalizing distal mass that is detrimental to the low inertia actuator's benefits.
3) When compared to the 6 DOF UR5 industry standard:
   a) a 6 DOF robot using nondelocalized, low inertia actuators like MR5 has a safety improvement of 1.6X (speed or force ratio);
   b) a 6 DOF robot using delocalized, low inertia actuators like Asimov has a safety improvement of 2.3X (speed or force ratio);

TABLE II
SPEED RATIO OF ALTERNATIVE ROBOTIC ARCHITECTURES

Architecture (3 DOF)	*Speed ratio*
Delocalized MR (Asimov)	*3.2*
MR5	*2.7*
Delocalized DC	*1.2*
UR5 (Reference)	*1.0*

Architecture (6 DOF)	*Speed ratio*
Delocalized MR (Asimov)	*2.3*
MR5	*1.6*
Delocalized DC	*1.1*
UR5 (Reference)	*1.0*

III. BAND-PASS FILTERING FOR SIMPLE COLLISION DETECTION

In addition to actuator architecture, the second necessary component of a safe interaction between robots and humans is a rapid, reliable, and simple contact detection method. Failure to achieve quick detection due to improper modeling with model-based collision detection methods, or due to a high level of complexity and lack of real-time performance when using vision algorithms or complex arrays of sensors, can compromise safety. To solve this problem, a simple and cost-effective collision detection method using only proprioceptive sensors already present on the robot (i.e., joint encoders) is implemented and tested on the Asimov MR actuator robot. The proposed method is similar to paper [31], without the need of computing in real-time an approximate dynamic model of the manipulator.

For an external disturbance force $\boldsymbol{F_{ext}}$ at the end-effector, the change in angular momentum $\boldsymbol{H}$ is as follows:

$$\Delta \boldsymbol{H} = \int_{t_o}^{t_{\text{impact}}} \boldsymbol{J(q)}^{\boldsymbol{T}} \boldsymbol{F_{ext}} dt = \int_{t_o}^{t_{\text{impact}}} \boldsymbol{\tau_{ext}} dt \qquad (15)$$

where t_o is the time at which the impact begins, t_{impact} is the time at which the impact ends, and $\tau_{\mathbf{ext}}$ is the vector of joint external torques resulting from the impact.

Assuming the position of the robot is almost constant during the impact, thus producing no significant changes in the manipulator inertia matrix, the variation of momentum can also be written as a function of the change of angular velocities

$$\Delta \boldsymbol{H} = \boldsymbol{M(q)} \Delta \dot{\boldsymbol{q}}. \qquad (16)$$

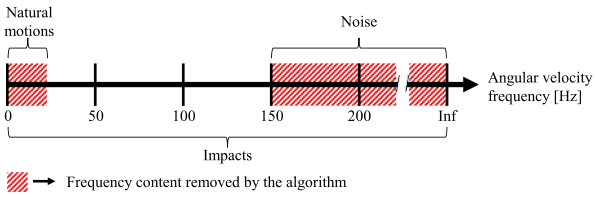

Fig. 10. Collision detection algorithm effects on the angular velocity frequency content.

And by combining (15) and (16), we obtain the following:

$$\Delta\dot{\boldsymbol{q}} = \boldsymbol{M}(\boldsymbol{q})^{-1} \int_{t_o}^{t_{\text{impact}}} \boldsymbol{\tau_{ext}} dt. \tag{17}$$

From (17), we can observe that it is challenging to use information from joint encoders to infer robot link dynamics and detect undesirable contacts when the inertia matrix is highly dominated by the contribution of the actuator, like with conventional servo-geared actuators. Indeed, the total inertia of the system is so high that collision forces only produce insignificant changes in angular velocities. In contrast, with MR actuators, total system inertia is at least one order of magnitude lower compared to a robot with a conventional stiff transmission, and collision forces can readily be detected since they will cause fast and large changes in angular velocities.

Generally, desirable robot movements stay within the range of 0 to 5 Hz with possible vibrations at higher frequencies. When an impact occurs, the mechanical structure of the robot is excited over a wide range of frequencies. However, the amplitudes of the resulting vibrations over 150 Hz are significantly attenuated, and the information collected by position sensors (e.g., encoders) over that threshold can be considered as noise (e.g., from electronics or signal processing). Therefore, the frequency content of the joint's angular velocities during impacts has content at high frequencies that are not present during the natural motion of the robot. The frequencies during normal operation are bounded by the torque bandwidth of the MR actuators (<30 Hz). It is then possible to use a bandpass filter on angular velocity signals to eliminate normal variations caused by the desired motion of the arm at low frequencies as well as high-frequency random noise to only keep the frequency content due to collisions. Spectral energy due to collision is isolated using a bandpass filter with high-pass and low-pass cutoff frequencies, respectively, of 30 Hz (1st order) and 150 Hz (1st order) as shown in Fig. 10. Each element of the filtered angular velocity vector is then compared to a normal variation threshold for a trajectory without collision. A signal exceeding this threshold for any joint triggers the detection signal.

Using a filtering detection algorithm offers two major advantages for MR-actuated robots.

1) It allows to detect when the robot is colliding with a human or an object, in any controllable direction of the robot, without the addition of expensive external sensors (i.e., joints torque sensors, accelerometers or instrumented skins).

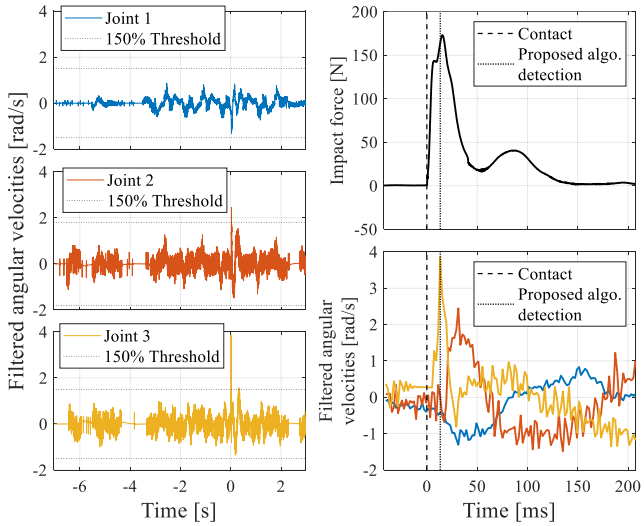

Fig. 11. Detection algorithm complete signal for a 10 s test including an impact (left), and end-effector force sensor (upper right), and detection signal (lower right) zoomed around contact time, for a contact of the end-effector with a nonclamped human hand at 1.5 m/s.

2) It avoids the difficulties of model-based contact detection methods such as the need for computationally intensive nonlinear models, the choice of the controller and the double differentiation of encoders to estimate angular acceleration.

The latter is almost always too noisy in practice to be observed without filtering out the frequencies of interest in collision situations [32].

The effectiveness of the frequency filtering detection algorithm when using MR actuators is verified by using the force sensor on the Asimov robot's effector to detect the initial impact to measure the algorithm's detection delay. Fig. 11 presents the end-effector force and the filtered angular velocity of each joint for a collision with a nonclamped human hand at 1.5 m/s. The nonclamped impact is used to validate the detection method in a worst-case situation since smaller perturbations are produced versus the clamped impact. Even with a large threshold set as 150% of the observed maximum of the normal variation measured for the same movements without collision, the detection of the algorithm is triggered quickly, only 10 ms after the contact.

Filtering detection can only have limited success when used with conventional manipulators due to actuators' high inertia that impedes sensitivity. The properties of MR-actuators overcome these limitations and are synergistic with bandpass filtering collision detection. The MR actuator's inertia is significantly lower than the robot links inertia and is less detrimental to sensitivity. Also, MR actuators are antagonistic in nature and have no backlash that could disrupt the velocity signal like an external impact, which can result in false detections.

A possible drawback of the detection method comes from removing the low-frequency content of the collision detection signal that can lead to not detecting low speed contact (deliberate or not). However, these contacts usually have a very low potential for danger and can still be detected with low bandwidth simple detection schemes, such as monitoring the position error.

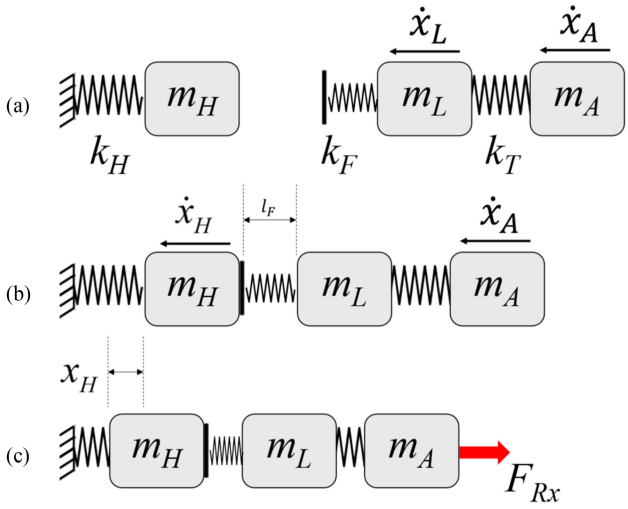

Fig. 12. 1-D collision model with foam padding and reaction force when masses are (a) preimpact, (b) at the instant of impact, and (c) postimpact where maximal force is reached.

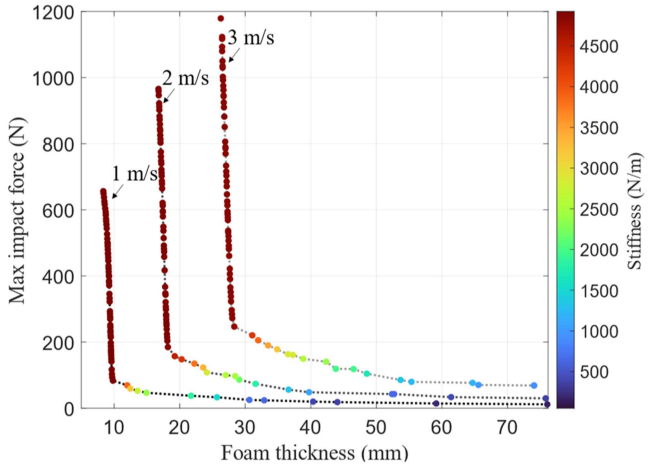

Fig. 13. Foam selection Pareto fronts for 1 DOF MR actuator at an impact speed of 1, 2, and 3 m/s.

IV. Foam Padding and Reflex Motion

When rigid contacts between human and robot happen, the maximum force value occurs within 10 ms after the beginning of the impact as seen in Fig. 5. This duration depends on the natural frequency of the impacted body part, determined by its mass and rigidity (hand's characteristics represent the most stringent case for contact duration). Even with the high bandwidth of the MR actuators (>30 Hz) and fast impact-detection sensors or algorithms, it is impossible to directly attenuate the initial force peak with an active reaction [25].

The scope of the work presented in this section is not to realize an exhaustive study on foam padding materials in robotics since a lot of literature already exists on the subject. The objective is to propose a major improvement in MR-actuated robot safety by using a passive layer of foam to separate the robot from the human to allow premature collision detection without large forces, thus enabling the actuator to actively react before the final rigid collision occurs. This layer of foam needs to be as soft as possible to attenuate the peak of the impact force and extend the duration of the impact but also to have a minimal stiffness to produce a perturbation large enough to detect contact before complete foam compression, thus increasing the available reaction time before rigid impact. This layer of foam should also be selected to minimize mechanical interference.

The selection of the foam padding can thus be framed as a multiobjective optimization problem where the objective is to minimize the impact force and the foam thickness. The two variable design parameters for a given robot are the foam stiffness (k_F) and uncompressed thickness (l_F). Using the compliant transmission model of Fig. 2 but adding a mass-less spring for the foam padding (see Fig. 12), it is possible to write the dynamic equations of motion for the human mass (m_H), the link mass (m_L) and the actuator mass (m_A) including the foam padding and reaction force F_{Rx} [see (18)–(20)]. The foam and human springs can only apply compressive forces.

The bandpass collision detection method is implemented on the link velocity $\dot{x}_L$ to trigger the reaction force applied on the actuator mass to retract from contact. The rise time of the reaction force is representative of the actuator bandwidth (i.e., not instantaneous). Complete foam compression is modeled by rapidly increasing k_F when the foam compression $(x_L - x_H)$ approaches the uncompressed foam thickness l_F

$$m_H\ddot{x}_H = k_F(x_L - x_H) - k_H x_H \tag{18}$$

$$m_L\ddot{x}_L = k_T(x_A - x_L) - k_F(x_L - x_H) \tag{19}$$

$$m_A\ddot{x}_A = -k_T(x_A - x_L) - F_{Rx}. \tag{20}$$

This model can then be used in dynamic simulations with different impact speeds ($\dot{x}_{L,0} = \dot{x}_{A,0} = v_{impact,0}$ and $\dot{x}_{H,0} = 0$) to evaluate the maximal impact force on human ($F_{H,\max} = \max(k_H x_H)$) for a given set of foam design parameters (k_F, l_F). The search of the optimal foam design parameters is performed using a multiobjective genetic algorithm (population of 200 design parameter sets, with 400 generations). The lower and upper bounds for the design parameters are 1) 50 N·m < k_F < 5000 N·m and 2) 3.2 mm < l_F < 76.2 mm to cover a wide range of stiffness and to represent foam thickness that could realistically be installed on a robot without mechanical interferences.

The two configuration of the 1 DOF test bench are used to compare the foam selection method for two representative actuators. The Pareto fronts that illustrate tradeoffs between force reduction and foam thickness for impacts at 1, 2, and 3 m/s are shown in Fig. 13 for the MR actuator and Fig. 14 for the dc actuator. The data points on the Pareto fronts are colored according to the optimal stiffness for a given foam layer thickness. Some general conclusions can be drawn from the following results:

1) A minimal thickness is needed to detect and react in a way that reduces the impact force before full compression. This thickness increases with the impact speed.
2) Important force reduction can be done once that minimal thickness is reached with little increase in foam thickness.

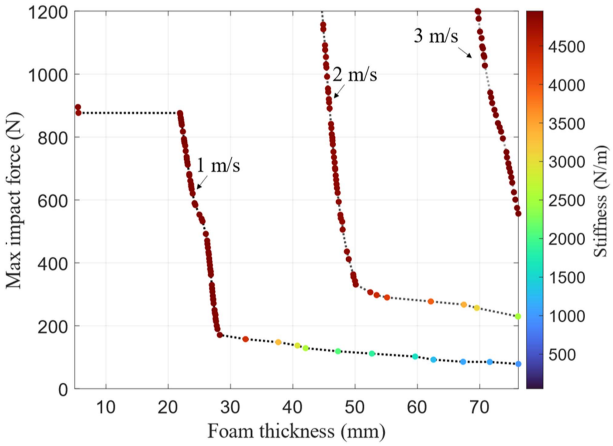

Fig. 14. Foam selection Pareto fronts for 1 DOF dc actuator at an impact speed of 1, 2, and 3 m/s.

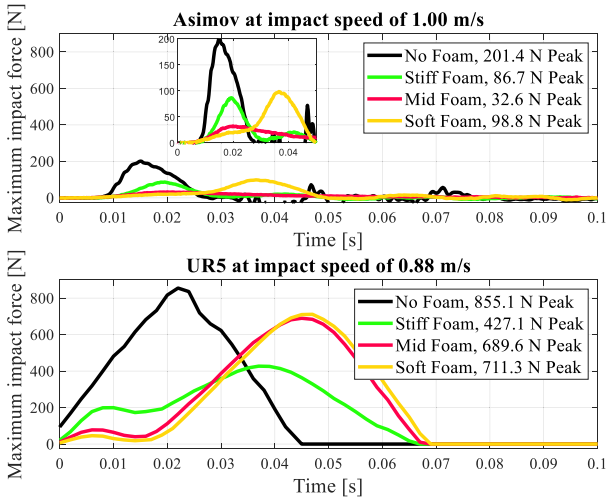

Fig. 15. Effect of 1 in of foam padding on maximum impact force reduction for (a) Asimov at 1.0 m/s and (b) UR5 at 0.88 m/s.

3) The slope of the Pareto fronts over a given thickness reduces considerably (e.g., in the range of 30–40 mm for the MR actuator). It means that adding thicker soft foam would not produce any considerable impact force reduction.
4) The Pareto fronts of the dc actuators show that the thickness of the foam layer must be significantly higher to start having benefits. For an impact of 3 m/s, the data points on the Pareto front exceeds the upper bound of foam thickness that was set as prohibitive (76 mm).

Ultimately, the selection of the foam padding is a tradeoff between the reduction of impact force and foam thickness that depends on the robot's task requirements (e.g., robot speed and mechanical interference). In that sense, the Pareto fronts provide useful information to robot designers to select an optimal foam. From a practical point of view, the foam strategy is difficult, if not impossible, to implement in robots using conventional actuators with high reflected inertia simply because the required thickness to get meaningful improvements in reaction time is prohibitive.

Experimentations on representative robots can be carried out to validate the effectiveness of the foam padding and reaction in reducing contact force for multi-DOF systems (Asimov and UR5 robots). The collision detection method of Section III is implemented on the Asimov robot, with a reflex motion to return to the position recorded 50 ms before the impact. As mentioned previously, this position is known to be safe and might be chosen differently in a real application to avoid any secondary impact. The main objective of the reflex motion is to show that it is possible to react fast enough to actively reduce the impact force with the contribution of the high torque bandwidth and the delay provided by the early detection enabled with foam padding when a safe post-impact position is known. As for the UR5, the built-in collision detection scheme with brake reaction is used.

Fig. 15 shows experimental results of the reduction in contact force perceived by the human hand for impacts performed by the Asimov and the UR5 robots with 25 mm thick sheets of flexible polyurethane foam. Three different foam stiffnesses were tested, soft, medium, and stiff foams with 25% compression reached under pressures of 1.4 kPa ($k_F = 150$ N·m) 2.8 kPa ($k_F = 300$ N·m), and 5.5 kPa ($k_F = 600$ N·m), respectively. End-effector speeds at contact are set to 1.0 and 0.88 m/s for the Asimov and UR5, respectively.

Results show important benefits when using foam layers with Asimov but not so much with the UR5. Indeed, a contact force reduction of more than 6X is observed with the medium stiffness foam for Asimov, while a reduction of only 2X is found for the UR5 with the stiff foam. Results also show that foam stiffness must be carefully selected for a given robot, impact speed, and impact detection strategy. For Asimov, the softer foam is too soft to allow contact detection while the stiffer foam is too stiff to produce many benefits. For the UR5, the two softer foams are not able to trigger the collision detection algorithm before full compression and the stiffest foam absorbs part of the impact, but as limited benefits as the UR5 reaction speed is limited.

When looking at the best results of each robot, it is observed that the 3 DOF Asimov has a maximum contact force 13.1X lower than the 6 DOF UR5 while operating 1.14X faster, leading to a total safety improvement of 14.9X (speed or force ratio). Assuming that the 59% increase of contact force when adding a 3 DOF wrist to Asimov holds (see Section III), the safety improvement potential provided by MR actuators and actuator delocalization over conventional robot actuators mounted in serial chains is estimated to be 9.4X when using reasonable foam padding and reflex motion (up from 2.3X without) Using the same analysis framework, the safety improvement potential provided by MR actuators alone on a 6 DOF robot like MR5 is estimated to 6.4X when using foam padding and reflex motion (up from 1.6X without). In all, foam padding and reflex motion on an MR-actuated robot have the potential to further improve safety by a factor of ∼4X compared to the same MR robot without padding and reaction.

V. Opening

An attempt is made to push the available hardware to its physical limits to get a sense of the full potential of delocalized MR

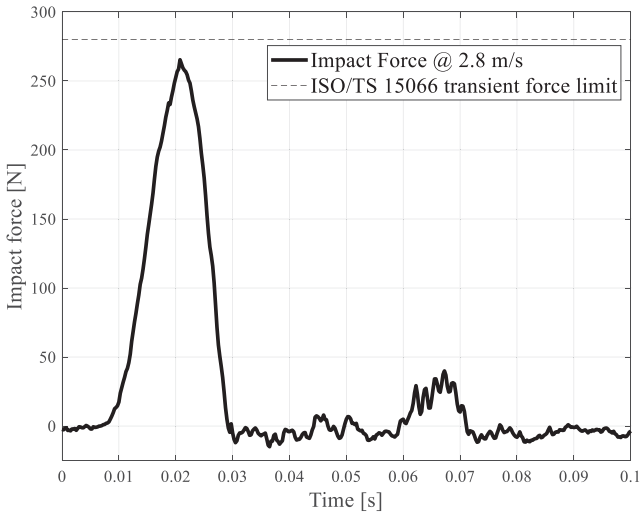

Fig. 16. Impact force profile at the maximal velocity reachable with Asimov and proposed integrated safety solution.

actuators with foam padding and reflex motion. The maximum speed of the 3 DOF Asimov is thus pushed to the test bench limit of 2.8 m/s. As shown in Fig. 16, the maximum contact force stays within the ISO/TS 15066 threshold for transient contact on the hand and finger (i.e., 280 N). Again, assuming that the 59% adjustment to bring Asimov to 6 DOF holds, we can estimate that a 6 DOF Asimov could operate safely at least at 1.75 m/s, which is 5.8X faster than the 6 DOF UR5, considered safe when operating at 0.3 m/s, as per the experimental data shown on Fig. 8.

VI. Conclusion

This article developed an experimentally validated model of collisions between robots and humans. This model shows that actuator inertia, and not actuator mass or location nor structural mass, is the dominating design parameter of current collaborative robots and must inevitably be minimized to gain significant performance and safety benefits. To this end, the low inertia MR actuators used in this study proved highly promising.

The collision model is validated on 1 DOF single joint devices as well as 3 and 6 DOF robots. The model is used to predict the safety performance of various relevant robot configurations. For 6 DOF robots, the model predicts that using low inertia MR actuators can increase safety by a factor of 1.6X over the current industry standard UR5 robot, and by a factor of 2.3X when using low inertia MR actuators and actuator delocalization.

Furthermore, the MR architecture allows the use of a fast and simple collision detection scheme based only on proprioceptive sensors, which was demonstrated experimentally. This detection method allows the avoidance of costly sensing hardware for collaborative robots, leading to a possible reduction in retail price.

This collision detection, coupled with an increased reaction time provided by foam padding, enables active force reduction increasing safety improvements up to 6.4X when using low inertia actuators only, and even further to 9.4X when using low inertia MR actuators and actuator delocalization. It opens the possibility of actively and intrinsically reducing the impact force of fast human-robot collisions with no need for external sensors, which to the authors' knowledge, has yet to be performed with conventional actuators.

Finally, pushing the hardware to its limits demonstrates that a 3 DOF robot with delocalized low inertia MR actuators and active force reduction can operate safely at 2.8 m/s while staying within the ISO/TS 15066 safety guidelines. This would correspond to a safety improvement of at least 5.8X over a UR5 on a 6 DOF MR robot.

Future works will develop full 6 DOF collaborative robots using MR actuators since such equipment is not yet available at this time. Delocalized as well as nondelocalized prototypes should be considered to fully understand the potential of each strategy. Such hardware will allow- to test the proposed collision model over its full operational envelope in terms of speed and DOFs and confirm its fidelity. Also, the collision detection and reflex motion approach presented in this article remain a proof-of-concept for collisions at the end-effector and should be generalized and improved to any contact anywhere on a robot with 6 DOF. Important features such as external force estimation and impact location identification will be developed using the same information from perturbation as used in the detection signal.

Acknowledgment

The authors would like to thank Exonetik and all the members of the Asimov project for financing, designing, and sharing the Asimov robot.

References

[1] L. Sanneman, C. Fourie, and J. A. Shah, "The state of industrial robotics: Emerging technologies, challenges, and key research directions," *Found. Trends® Robot.*, vol. 8, no. 3, pp. 225–306, Mar. 2021, doi: 10.1561/2300000065.

[2] J. Fryman and B. Matthias, "Safety of industrial robots: From conventional to collaborative applications," in *Proc. IEEE 7th German Conf. Robot.*, 2012, pp. 1–5.

[3] A. N. Link, Z. T. Oliver, and A. C. O'Connor, "Economic analysis of technology infrastructure needs for advanced manufacturing: Advanced robotics and automation," Nat. Inst. Standards Technol., Gaithersburg, MD, USA, NIST GCR 16-005, Oct. 2016, doi: 10.6028/NIST.GCR.16-005.

[4] M. Zinn, B. Roth, O. Khatib, and J. K. Salisbury, "A new actuation approach for human friendly robot design," *Int. J. Robot. Res.*, vol. 23, no. 4/5, pp. 379–398, Apr. 2004, doi: 10.1177/0278364904042193.

[5] N. Lauzier and C. Gosselin, "Series clutch actuators for safe physical human-robot interaction," in *Proc. IEEE Int. Conf. Robot. Automat.*, 2011, pp. 5401–5406, doi: 10.1109/ICRA.2011.5979601.

[6] T. Hull and M. A. Minarcin, "Considerations in collaborative robot system designs and safeguarding," *SAE Int. J. Mater. Manuf.*, vol. 9, no. 3, pp. 545–551, Aug. 2016, doi: 10.4271/2016-01-0340.

[7] J. Li, S. Li, S. Li, and X. Mao, "Tradeoff between safety and performance for humanoid rehabilitation robot based on stiffness," in *Proc. IEEE Int. Conf. Mechatron. Automat.*, 2017, pp. 1585–1590, doi: 10.1109/ICMA.2017.8016053.

[8] H.-S. Kim, I.-M. Kim, C.-N. Cho, and J.-B. Song, "Safe joint module for safe robot arm based on passive and active compliance method," *Mechatronics*, vol. 22, no. 7, pp. 1023–1030, Oct. 2012, doi: 10.1016/j.mechatronics.2012.08.007.

[9] G. A. Pratt and M. M. Williamson, "Series elastic actuators," in *Proc. IEEE/RSJ Int. Conf. Intell. Robots Syst.. Hum. Robot Interaction Cooperative Robots*, 1995, vol. 1, pp. 399–406, doi: 10.1109/IROS.1995.525827.

[10] L. Joseph, V. Padois, and G. Morel, "Online minimization of the projected mass of a robot for safe workspace sharing with a human," in *Proc. IEEE Int. Conf. Robot. Automat.*, Montreal, Canada, May 2019.
[11] V. Duchaine, N. Lauzier, M. Baril, M.-A. Lacasse, and C. Gosselin, "A flexible robot skin for safe physical human robot interaction," in *Proc. IEEE Int. Conf. Robot. Automat.*, 2009, pp. 3676–3681. doi: 10.1109/ROBOT.2009.5152595.
[12] S. Haddadin, A. Albu-Schaffer, A. De Luca, and G. Hirzinger, "Collision detection and reaction: A contribution to safe physical human-robot interaction," in *Proc. IEEE/RSJ Int. Conf. Intell. Robots Syst.*, 2008, pp. 3356–3363, doi: 10.1109/IROS.2008.4650764.
[13] A. Caldas, M. Makarov, M. Grossard, P. Rodriguez-Ayerbe, and D. Dumur, "Adaptive residual filtering for safe human-robot collision detection under modeling uncertainties," in *Proc. IEEE/ASME Int. Conf. Adv. Intell. Mechatron.*, 2013, pp. 722–727, doi: 10.1109/AIM.2013.6584178.
[14] A. Luca, A. Albu-Schaffer, S. Haddadin, and G. Hirzinger, "Collision detection and safe reaction with the DLR-III lightweight manipulator arm," in *Proc. IEEE/RSJ Int. Conf. Intell. Robots Syst.*, 2006, pp. 1623–1630, doi: 10.1109/IROS.2006.282053.
[15] *Robots and Robotic Devices - Collaborative Robots*, Standard ISO/TS 15066:2016(en), 2016.
[16] A. S. Shafer and M. R. Kermani, "On the feasibility and suitability of MR fluid clutches in human-friendly manipulators," *IEEE/ASME Trans. Mechatron.*, vol. 16, no. 6, pp. 1073–1082, Dec. 2011, doi: 10.1109/TMECH.2010.2074210.
[17] J. Viau, P. Chouinard, J.-P. L. Bigue, G. Julio, F. Michaud, and J.-S. Plante, "Tendon-driven manipulator actuated by magnetorheological clutches exhibiting both high-power and soft motion capabilities," *IEEE/ASME Trans. Mechatron.*, vol. 22, no. 1, pp. 561–571, Feb. 2017, doi: 10.1109/TMECH.2016.2605379.
[18] P. Chouinard, M. Denninger, and J.-S. Plante, "Reliable and lightweight primary flight control actuation using magneto-rheological clutches in slippage," in *Proc. IEEE Int. Conf. Robot. Automat.*, 2015, pp. 213–219, doi: 10.1109/ICRA.2015.7139002.
[19] M.-A. Bégin et al., "Experimental assessment of a controlled slippage magnetorheological actuator for active seat suspensions," *IEEE/ASME Trans. Mechatron.*, vol. 23, no. 4, pp. 1800–1810, Aug. 2018, doi: 10.1109/TMECH.2018.2836351.
[20] C. Véronneau, J.-P. Lucking Bigué, A. Lussier-Desbiens, and J.-S. Plante, "A high-bandwidth back-drivable hydrostatic power distribution system for exoskeletons based on magnetorheological clutches," *IEEE Robot. Automat. Lett.*, vol. 3, no. 3, pp. 2592–2599, Jul. 2018, doi: 10.1109/LRA.2018.2812910.
[21] C. Khazoom, C. Veronneau, J.-P. L. Bigue, J. Grenier, A. Girard, and J.-S. Plante, "Design and control of a multifunctional ankle exoskeleton powered by magnetorheological actuators to assist walking, jumping, and landing," *IEEE Robot. Automat. Lett.*, vol. 4, no. 3, pp. 3083–3090, Jul. 2019, doi: 10.1109/LRA.2019.2924852.
[22] C. Véronneau et al., "Modular magnetorheological actuator with high torque density and transparency for the collaborative robot industry," *IEEE Robot. Automat. Lett.*, vol. 8, no. 2, pp. 896–903, Feb. 2023, doi: 10.1109/LRA.2022.3231524.
[23] P. Yadmellat, A. S. Shafer, and M. R. Kermani, "Design and development of a single-motor, two-DOF, safe manipulator," *IEEE/ASME Trans. Mechatron.*, vol. 19, no. 4, pp. 1384–1391, Aug. 2014, doi: 10.1109/TMECH.2013.2281598.
[24] A. Bicchi et al., "Physical human-robot interaction: Dependability, safety, and performance," in *Proc. IEEE 10th Int. Workshop Adv. Motion Control*, 2008, pp. 9–14, doi: 10.1109/AMC.2008.4516033.
[25] S. Haddadin, "Towards safe robots," in *Springer Tracts in Advanced Robotics*, vol. 90. Berlin, Germany: Springer, 2014, doi: 10.1007/978-3-642-40308-8.
[26] UAW Health and Safety Department, "Review of robot injuries - one of the best kept secrets," in *Proc. Nat. Robot Conf.*, 2004, pp. 1647–1653.
[27] O. Khatib, "Inertial properties in robotic manipulation: An object-level framework," *Int. J. Robot. Res.*, vol. 14, no. 1, pp. 19–36, Feb. 1995, doi: 10.1177/027836499501400103.
[28] M. Budinger, J. Liscouët, F. Hospital, and J.-C. Maré, "Estimation models for the preliminary design of electromechanical actuators," *Proc. Inst. Mech. Engineers, Part G, J. Aerosp. Eng.*, vol. 226, no. 3, pp. 243–259, Mar. 2012, doi: 10.1177/0954410011408941.
[29] S.-D. Lee, B.-S. Kim, and J.-B. Song, "Human–robot collision model with effective mass and manipulability for design of a spatial manipulator," *Adv. Robot.*, vol. 27, no. 3, pp. 189–198, Mar. 2013, doi: 10.1080/01691864.2012.754076.
[30] M. Gervais, L.-P. Lebel, and J.-S. Plante, "Design exploration and experimental characterization of a 6 degrees-of-freedom robotic manipulator powered by cable-driven semi-delocalized magnetorheological actuators," in *Proc. Int. Conf. Robot. Automat.*, Philadelphia, PA, USA, 2022, pp. 11416–11423, doi: 10.1109/ICRA46639.2022.9812275.
[31] B. Jung, J. C. Koo, H. R. Choi, and H. Moon, "Human-robot collision detection under modeling uncertainty using frequency boundary of manipulator dynamics," *J. Mech. Sci. Technol.*, vol. 28, no. 11, pp. 4389–4395, Nov. 2014, doi: 10.1007/s12206-014-1006-5.
[32] S. Haddadin, A. D. Luca, and A. Albu-Schäffer, "Robot collisions: A survey on detection, isolation, and identification," *IEEE Trans. Robot.*, vol. 33, no. 6, pp. 1292–1312, Dec. 2017, doi: 10.1109/TRO.2017.2723903.

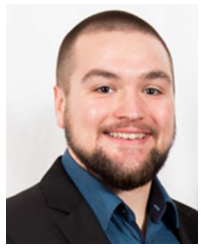

Alexandre St-Jean received the B.Sc.A. degree in mechanical engineering from the Université de Sherbrooke, Sherbrooke, QC, Canada, in 2017. He is currently working toward the Ph.D. degree in control and design of safe and performant robots using magnetorheological actuators with Université de Sherbrooke, Sherbrooke, QC, Canada.

He is currently a member of the CREATEK laboratory team. His current research interests include control and mechanical design of safe and performant robots and dynamic systems modeling.

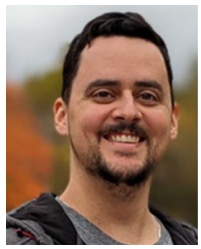

Francis Dorval received the B.Sc.A. degree in mechanical engineering from the Université de Sherbrooke, Sherbrooke, QC, Canada, in 2020.

His research interests include mechanical design and instrumentation of robotic and sport equipment. He is currently a Candidate to the Mechanical Engineering in a robotic hardware company.

Jean-Sébastien Plante received the B.Sc.A. and M.Sc.A. degrees in mechanical engineering from the Université de Sherbrooke, Sherbrooke, QC, Canada, in 1998 and 2001, respectively, and the Ph.D. degree from the Massachusetts Institute of Technology (MIT), Cambridge, MA, USA, in 2006.

In 2007, he was an Associate Professor with the Department of Mechanical Engineering, Université de Sherbrooke, where he co-founded the CREATEK laboratory, a laboratory dedicated to the development of various new technological innovations. His current research interests in mechatronics include high-energy and power-density actuators based on magnetorheological fluid.

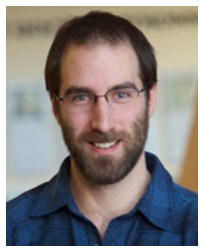

Alexis Lussier-Desbiens received the B.Sc.A. degree in mechanical engineering from the Université de Sherbrooke, Sherbrooke, QC, Canada, in 2005, and the Ph.D. degree in UAV landing and perching on vertical surfaces from Stanford University, Stanford, CA, USA, in 2012.

In 2013, he was an Associate Professor with the Department of Mechanical Engineering, Université de Sherbrooke, where he cofounded the CREATEK laboratory, a laboratory dedicated to the development of various new technological innovations. At Sherbrooke, he now works on developing technologies for long duration aquatic-aerial operations, tree-sampling, scansorial-aerial locomotion, robust UAV landing on moving platforms, sports equipment engineering, and safe high performance robotic arms.